Supporting Information

Strengthened d-p orbital hybridization and hydrogen diffusion in a hollow N-doped porous carbon/Ru cluster catalyst system for hydrogen evolution reactions

Ruidong Li, Hongyu Zhao, Lin Wang, Qingqu Zhou, Xiong Yang, Linbo Jiang, Xu Luo, Jun Yu, Jingwen Wei, Shichun Mu

Experimental Details

1.1 Chemicals and materials

Zirconium (IV) chloride ($ZrCl_4$, >99.9%), 2-aminoterephthalic acid (NH_2-H_2BDC, >99.9%), acetic acid (AR, 99.5%) and propionic acid (AR, 99.5%) were provided by Aladdin Industrial Co., China. Ruthenium(III) chloride ($RuCl_3$, 45-55%) was gained from Rhawn Reagent Co., Ltd. Dodecane (99%) and potassium chloride (KCl) were purchased by Sinopharm Chemical Reagent Co. Commercial Pt/C catalyst (20%) and Nafion solution (5%) were acquired from Sigma-Aldrich Chemical Reagent Co., Ltd. All reagents were used without further purification.

1.2 Materials Syntheses

1.2.1 Synthesis of the H-UiO-66-NH_2

First, 2-aminoterephthalic acid (NH_2-H_2BDC) (90.5 mg, ~0.5 mmol) and $ZrCl_4$ (116 mg, ~0.5 mmol) were dispersed in a mixture of acetic acid (6 mL) and deionized water (9 mL), then stirred at 90 °C for 24 h, and finally cooled to room temperature. The brown powder was obtained by centrifugation, washed sequentially with deionized water and ethanol, and then dried in vacuum at 100 °C. Second, 100 mg of IL-UiO-66-NH_2 was dispersed into 11 mL of H_2O/propionic acid (PA) (4/3, v/v) using ultrasound to obtain a homogeneous mixture. The mixture was transferred to and heated in a 25 mL Teflon autoclave at 100 °C for 6 h. After slowly cooling to ambient temperature, the formed precipitate was washed three times with H_2O and ethanol and dried overnight under vacuum to obtain hollow UiO-66-NH_2 (H-UiO-66-NH_2) as a brown powder.

1.2.2 Synthesis of H-ZrO_2/NC, H-NPC, ZrO_2/NC and NPC

To obtain the hollow nano derived carbon material, the powder of H-UiO-66-NH_2 was heated to 850 °C at the rate of 5 °C/min in a tube furnace under the argon atmosphere and then maintained for 3 h. The obtained black powder with hollow structure was denoted as H-ZrO_2/NC. Furthermore, the H- ZrO_2/NC was suspended in an aqueous solution of hydrofluoric acid (10 wt%) for 12 h and washed by deionized

water, then the resulted black powder (named as H-NPC) was collected by centrifugation and finally dried under vacuum. Similarly, the synthesis of ZrO_2/NC and NPC corresponds with the aforementioned methods accordingly.

1.2.3 Synthesis of c-Ru@H-NPC and c-Ru@NPC catalysts

Loading of Ru clusters on various materials was accomplished by using a double solvent approach. Taking the synthesis of c-Ru@H-NPC as an example, 15 mg of $RuCl_3$ was dispersed in ethanol solution (5 mL) and the solution was stirred at room temperature for 2 h. H-NPC (30 mg) was pre-activated by heating at 60 °C, followed by dropwise addition of aqueous $RuCl_3$ solution with continuous stirring for 12h. The powder obtained by filtration was dried in air at room temperature and then heated to 350°C for 3 h under a reducing atmosphere of 10% H_2/Ar to achieve c-Ru@H-NPC. The c-Ru@NPC was also prepared with a similar procedure to that of c-Ru@H-NPC, but using solid NPC instead of H-NPC.

1.3 Characterization

Morphologies and structures of c-Ru@H-NPC and other catalysts were recorded by Hitachi S-4800 and JEOL-2100F instruments. The high-angle annular dark field (HAADF) and energy-dispersive X-ray spectroscopy (EDS) elemental mapping images were conducted using EDAX Genesis. BET surface area analysis was performed at 77 K using an automatic volumetric adsorption analyzer Tristar II 3020. X-ray characterization of the catalysts was performed at room temperature with Cu Kα radiation (D8 Advance, Bruker, λ=1.5418 Å). XPS experiments were performed on a PHI Quantera X-ray photoelectron spectrometer. X-ray absorption spectra were recorded in fluorescence mode (Ru K-edge) with the beamline of Shanghai Synchrotron Light Source. Inductively coupled plasma-mass spectrometry (ICP-AES, Prodigy7) was performed to determine the actual metal content of various catalysts. The PHI Quantera X-ray photoelectron spectrometer was used for XPS experiments.

1.4 Catalytic reaction

All the electrocatalytic measurements of the catalysts were evaluated in an electrochemical workstation (CHI660E) as three-electrode system, except the analysis of overall water splitting using the two-electrode system. Glassy carbon (GC) electrode, graphite rod and Hg/HgO was served as the working electrode, counter electrode and reference electrode, respectively. The electrolytes were 1 M potassium hydroxide (KOH) and alkaline seawater (1 M KOH + seawater) solutions.

Preparation of alkaline seawater: Dissolve 6.6 g of KOH in 100 ml of seawater and stir for ten minutes, then centrifuge the supernatant once and stir for another 6 h to obtain the alkaline seawater.

The catalyst ink was fabricated by dispersing 5 mg of the as-prepared sample and 1 mg of conductive XC-72 powder into a mixture containing 440 μL isopropyl alcohol, 50 μL water, and 10 μL 5% Nafion solution. Then, the black mixture was ultrasonically dispersion for 30 minutes. Afterward, 2.5 μL of the ink was coated on the GC electrode with a diameter of 3 mm and dried under an infrared lamp to obtain the catalyst layer

with a loading of 0.354 mg cm^{-2}. Similarly, the commercial catalyst of 20 wt% Pt/C was dispersed into the same mixture, 2.5 µL ink was loaded onto the GC electrode with the same mass loading afterward.

For the hydrogen evolution reaction (HER), linear sweep voltammetry (LSV) was conducted with a scan rate of 5 mV s^{-1}. All polarization curves were iR-corrected. The electrochemical impedance spectroscopy (EIS) was conducted at the corresponding potentials of 10 mA cm^{-2} from LSV curves, with a frequency range of 0.01 to 100 000 Hz at −0.026 V vs. RHE. The double-layer capacitance (Cdl) was determined by recording cyclic voltammetry curves in the non-reactive region with a scan rate of 20 to 100 mV s^{-1}. The Cdl was calculated using the formula Cdl = ΔJ/2v, where ΔJ represents the current density difference and v represents the scan rate. The electrochemical specific surface area (ECSA) was calculated using the formula ECSA = Cdl/Cs, where Cs is the specific capacitance for an ideal flat surface (the real surface area was 1 cm^2). In this study, a general value of 60 µF cm^{-2} was adopted for Cs. Durability tests can be assessed using CV accelerating tests (0.024–-0.176 V vs. RHE) and chronoamperometry tests at 10 mA cm^{-2} on a glassy carbon electrode was also -0.026 V vs. RHE.

Mass activity calculation: Mass activity (j_{mass}) is often used to compare the intrinsic activity of different catalysts, determined using the following equation:

$$j_{mass} = \frac{j_{geo}(A\ cm^{-2})}{m_{loading} \times Ru\ wt\%\ (g\ cm^{-2})}$$

where j_{geo} is the geometric current density obtained from the three-electrode system with glassy carbon as the working electrode, m_{loading} is the loading of catalysts on the GCE and Ru wt% is the mass ratio of Ru in catalysts based on ICP results.

1.5 Finite-element method simulations

Two single-particle models were established based on the microstructure. The octahedron was based on SEM and TEM images that defined an open-pore structure for the hollow c-Ru@H-NPC particles, in which the edge length is 95 nm, the height is 150 nm, and the thickness of the hollow structure is 25 nm. c-Ru@NPC is a solid structure with similar dimensions to c-Ru@H-NPC. The dimensions of bulk c-Ru@NPC particles matched those of the hollow particles. Modeling and meshing were performed using the COMSOL Multiphysics finite-element solver.

Porous media mass transfer module：

$$\varepsilon \frac{\partial c}{\partial t} + \nabla \cdot \mathbf{J} = R$$

$$\mathbf{J} = -D_e \nabla c$$

c is the mass transfer fluid concentration, J is the mass transfer flux, ε is the porosity (0.64), R is the reaction source, representing the catalytic reaction occurring

at the surface, De is the fluid mass transfer coefficient (10-8[m2/s]) in porous media, and the porous media mass transfer satisfies the Milington-Quirk model. The catalytic reaction exists on both the surface and the interior of the hollow model, and the reaction occurs only on the surface of the solid model.

$$D_e = \frac{\varepsilon}{\varepsilon^{-\frac{1}{3}}} D_c$$

Dc is the diffusion coefficient of the fluid itself.

1.6 Computational Details

The Density functional theory (DFT) calculations were conducted in the Vienna Abinitio Simulation Package (VASP). The electron exchange and correlation energy were treated with the Perdew-Burke-Ernzerhof (PBE) functional within the generalized gradient approximation (GGA).[1-2] The ion cores-valence electrons interactions were described through the projected augmented wave (PAW) means, and the van der Waals interactions were eliminated with Grimme's method.[3] The simulations were implemented with a plane-wave basis set defined by a kinetic energy cutoff of 400 eV, and a 2×2×1 Monkhorst Pack k-point grid was used to integrate the Brillouin zone.[4-5] The geometry optimization and energy calculation were terminated when the electronic self-consistent iteration and force reached 10-5 eV and 0.02 eV Å-1, respectively. As for the construction of c-Ru@H-NPC model, an N-doped C support with non-periodic boundary was applied to present the H-NPC. Along all directions, we posed vacuum space of 10 Å to avoid interactions. The composite model of c-Ru@H-NPC was constructed by loading the Ru12 cluster model onto the N-doped C support model (86 C, 6 N, 12 Ru atoms). The adsorption behaviors of various key reaction intermediates in HER were investigated to evaluate the theoretical catalytic activity.

The calculation model of Ru/C was constructed by loading the Ru12 cluster model onto the crystalline N-doped C model (92 C, 12 Ru atoms). A vacuum space as large as 15 Å was used along the c direction to avoid periodic interactions. The k-point sampling was obtained from the Monkhorst-Pack scheme with a (2×2×1) mesh for optimization and a (2×2×1) mesh for calculations of electronic structure.

Bulk Ru models were built from Ru (101) lattice plane. The supercell with a lattice constant of 9.76 × 8.41 Å2 is consisted of 48 Ru atoms within 4 layers. The k-point sampling was obtained from the Gamma scheme with a (3×3×1) mesh for optimization and a (5×6×1) mesh for the calculations of electronic structure.

The alkaline HER reaction could be divided into two elementary reactions:

$$H_2O + e^- + * = *H + OH^*$$

$$H = * + 1/2\ H_2$$

Where *H signifies the H moiety on the adsorption site. The energy of H+/e- is approximately equal to the energy of 1/2 H2. The change in Gibbs free energy (ΔG) of

each adsorbed intermediate was calculated according to the computational hydrogen electrode method developed by Nørskov et al.[6] At standard conditions (T = 298.15 K, pH = 0, and U = 0 V (vs. SHE)), the free energy is defined as the following equation:

$$\Delta G = \Delta E + \Delta EZPE - T\Delta S$$

Where ΔE represents the energy change obtained from DFT calculation, ΔEZPE is the difference between the adsorbed state and gas, which is calculated by summing vibrational frequency for all model based on the equation: EZPE = 1/2∑hVi . T is the temperature (298.15 K) in the above reaction system, and ΔS represents the difference on the entropies between the adsorbed state and gas phase. The entropies of free molecules were obtained from NIST database (https://janaf.nist.gov/). And the free energy of the adsorbed state *H can be taken as: ΔG*H = ΔE*H + 0.24.[7]

The d-band center proposed by Nørskov and co-workers is a semi-quantitative descriptor to describe the trend of reactivity of transition metals (TM), which is defined the d-band center (εd) relative to the Fermi level (EF).[8] A transition metal with a low εd value relative to the Fermi level, shows a weak adsorption for a given adsorbate. And the d-band center (εd) was calculated as follows:

$$\varepsilon_d = \frac{\int_{-\infty}^{+\infty} x\rho(x)\mathrm{d}x}{\int_{-\infty}^{+\infty} \rho(x)\mathrm{d}x}$$

Where ρ(x) is the projector density of states (PDOS) with respect to N and Ru atom on Ru, carbon, and N-doped carbon models. Among them, we calculated the d-band center of average N sites, C sites and average Ru sites.

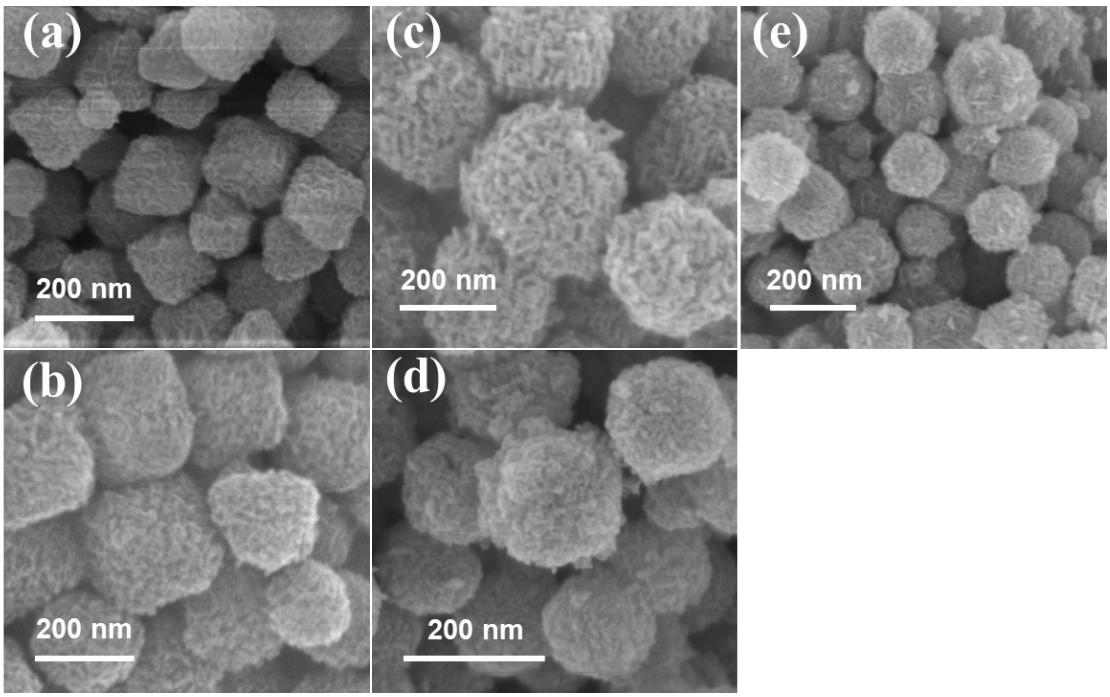

Figure S1. The SEM image of ZrO_2/NC (a), NPC (b), UiO-66-NH_2 (c), H-ZrO_2/NC (d) and H-NPC(e)

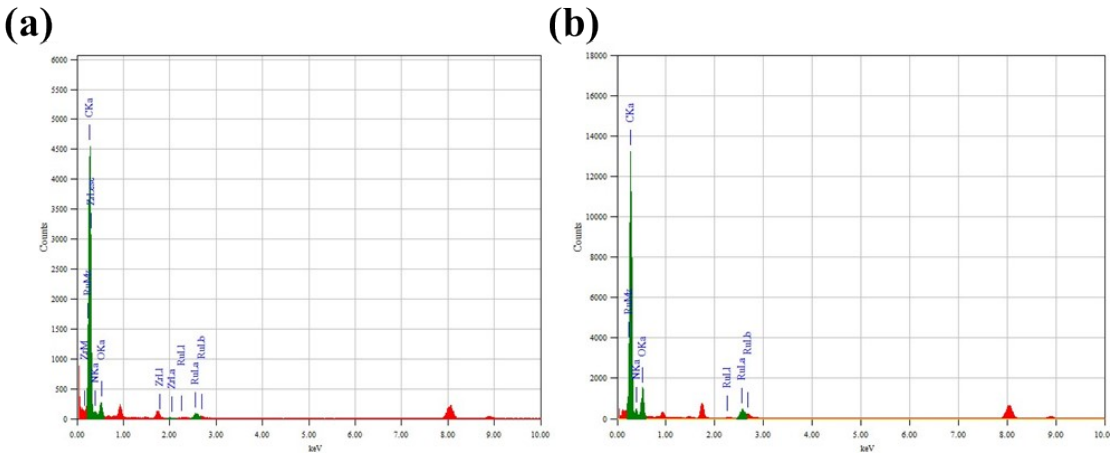

Figure S2. Atomic fraction of c-Ru@H-NPC(a) and c-Ru@NPC (b).

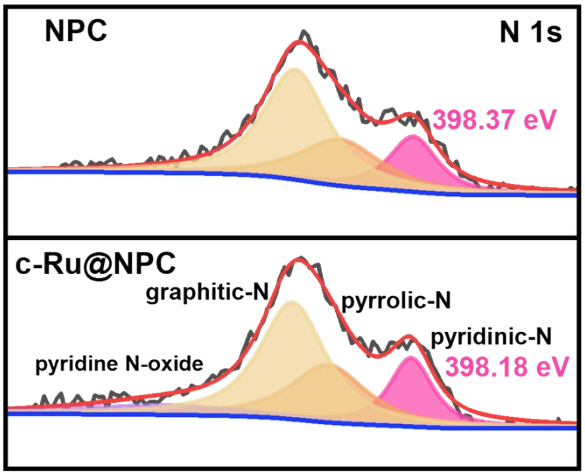

Figure S3. The high-resolution N 1s XPS spectra of NPC and c-Ru@NPC.

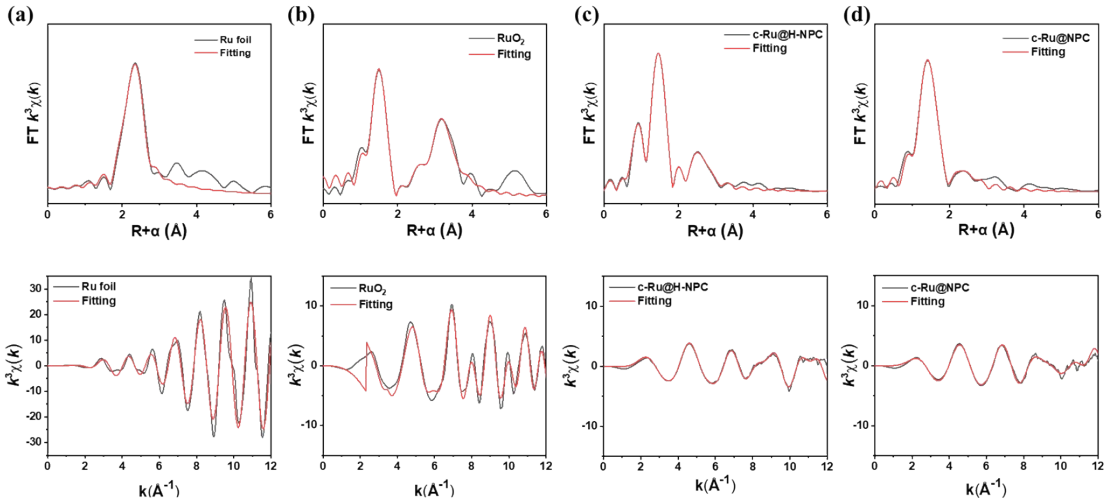

Figure S4. Fitting results of EXAFS spectra in R-space and k-space for (a) Ru foil, (b) RuO_2, (c) c-Ru@H-NPC and (d) c-Ru@NPC.

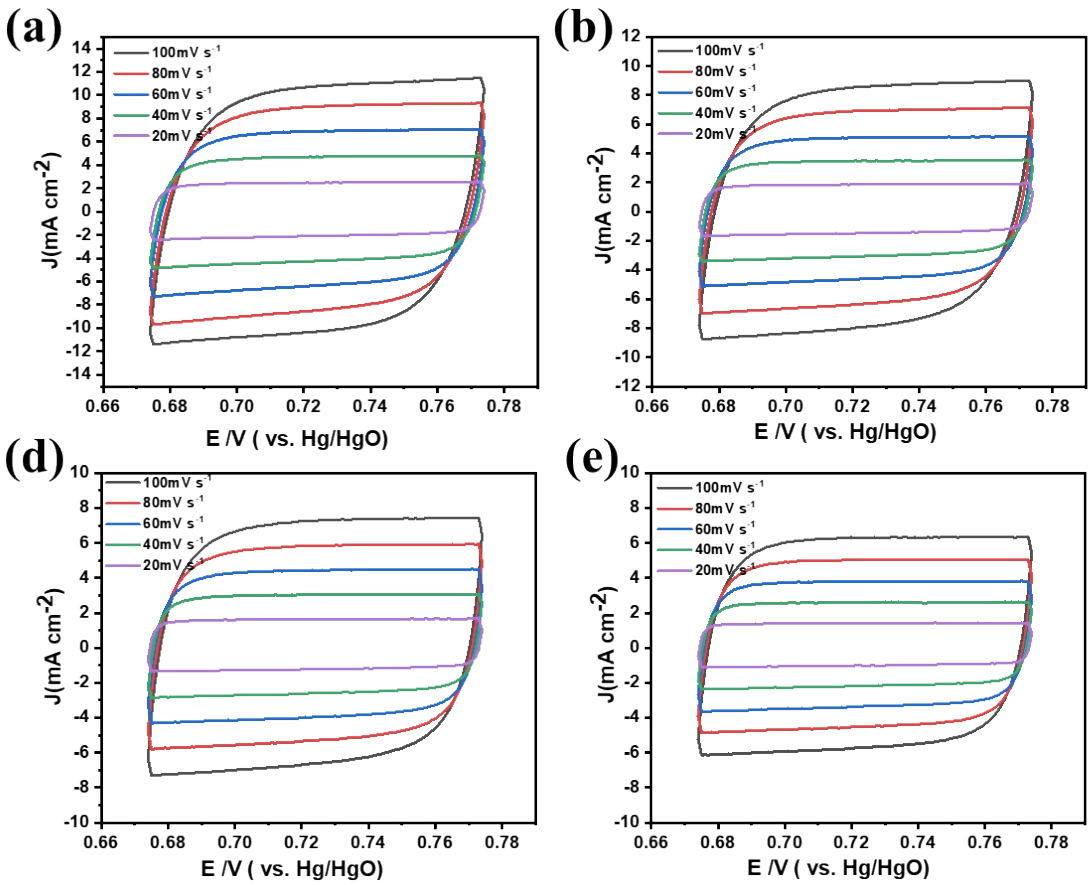

Figure S5. CV curves outside the neutral HER region of (a) c-Ru@H-NPC; (b) c-Ru@NPC; (c)H-NPC and (d) NPC in 1 M KOH.

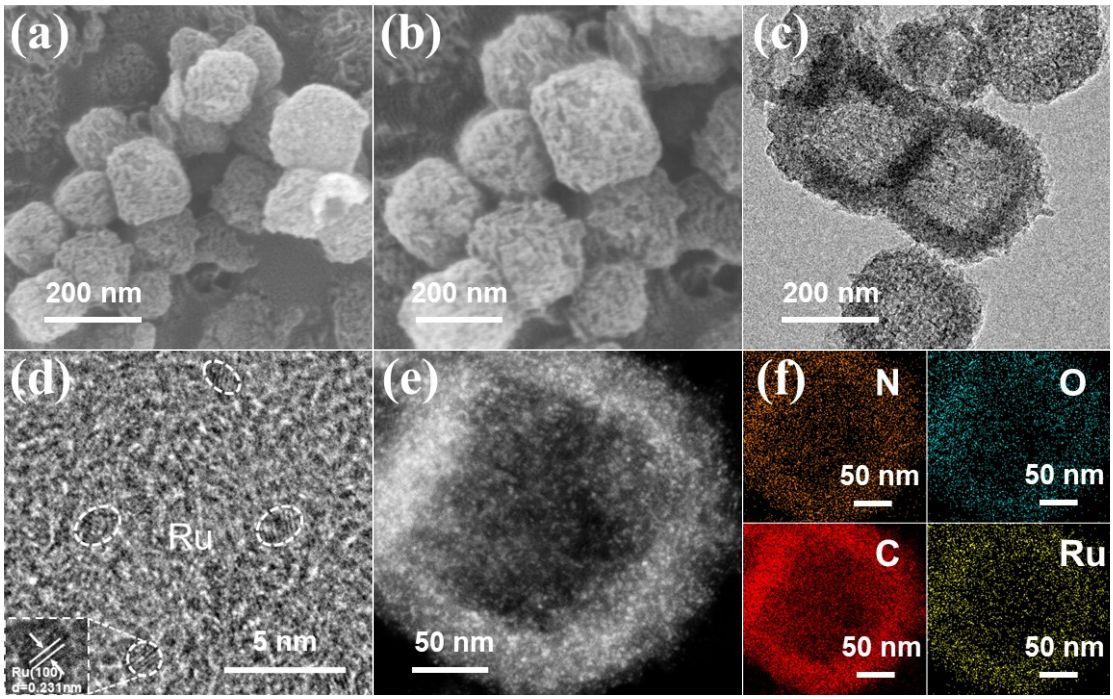

Figure S6. (a-b) SEM image of used c-Ru@H-NPC; (c) TEM images of used c-Ru@H-NPC; (d) High resolution TEM images of used c-Ru@H-NPC; (e-f) HAADF-STEM image of c-Ru@H-NPC after HER test and the corresponding EDS elemental mappings of Ru, C, N and O.

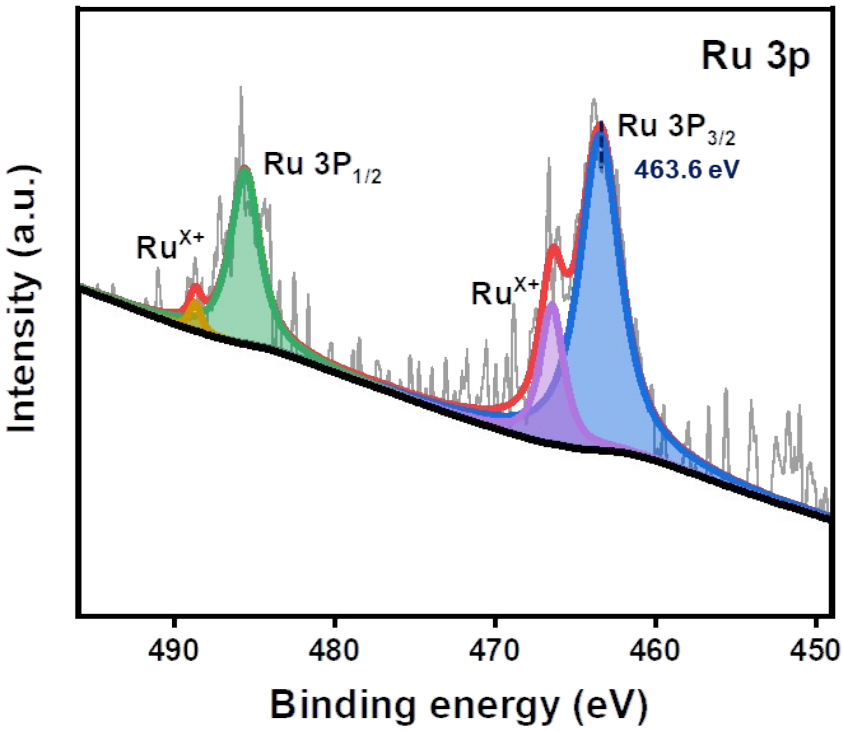

Figure S7. The Ru 3p spectra of used c-Ru@H-NPC.

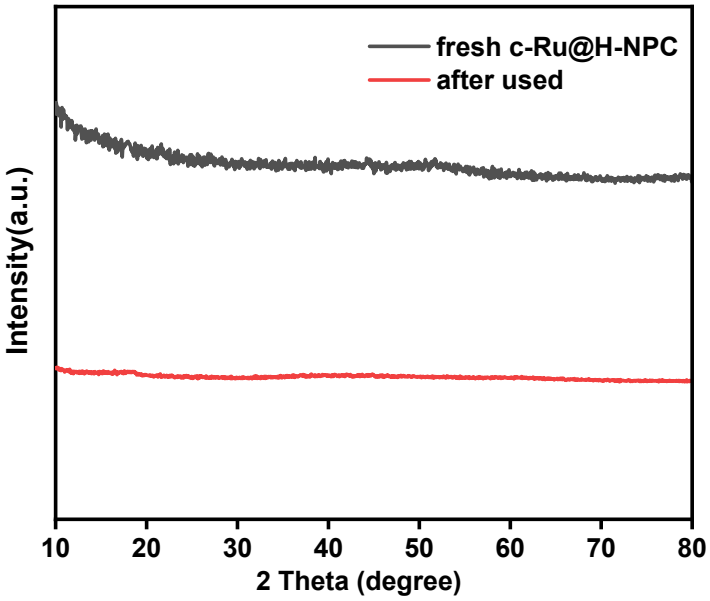

Figure S8. XRD patterns of c-Ru@H-NPC after HER test.

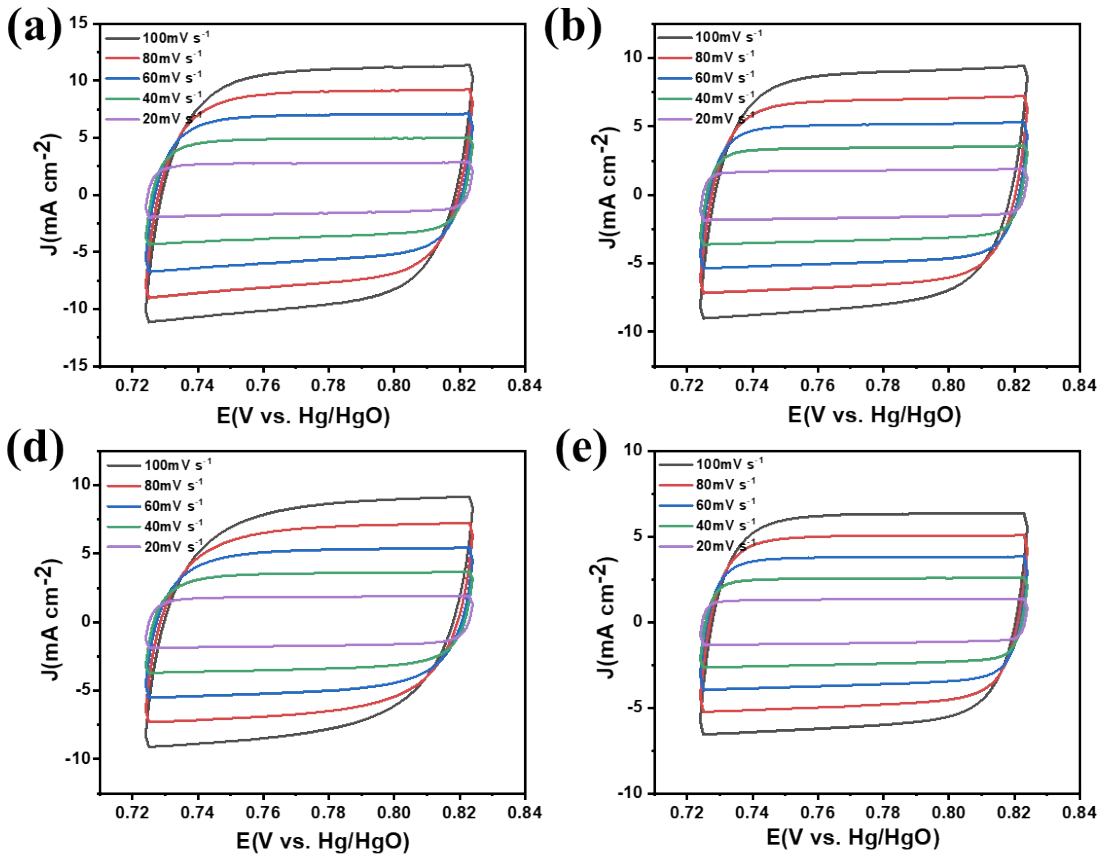

Figure S9. CV curves outside the neutral HER region of (a) c-Ru@H-NPC; (b) c-Ru@NPC; (c) H-NPC and (d) NPC in simulated seawater.

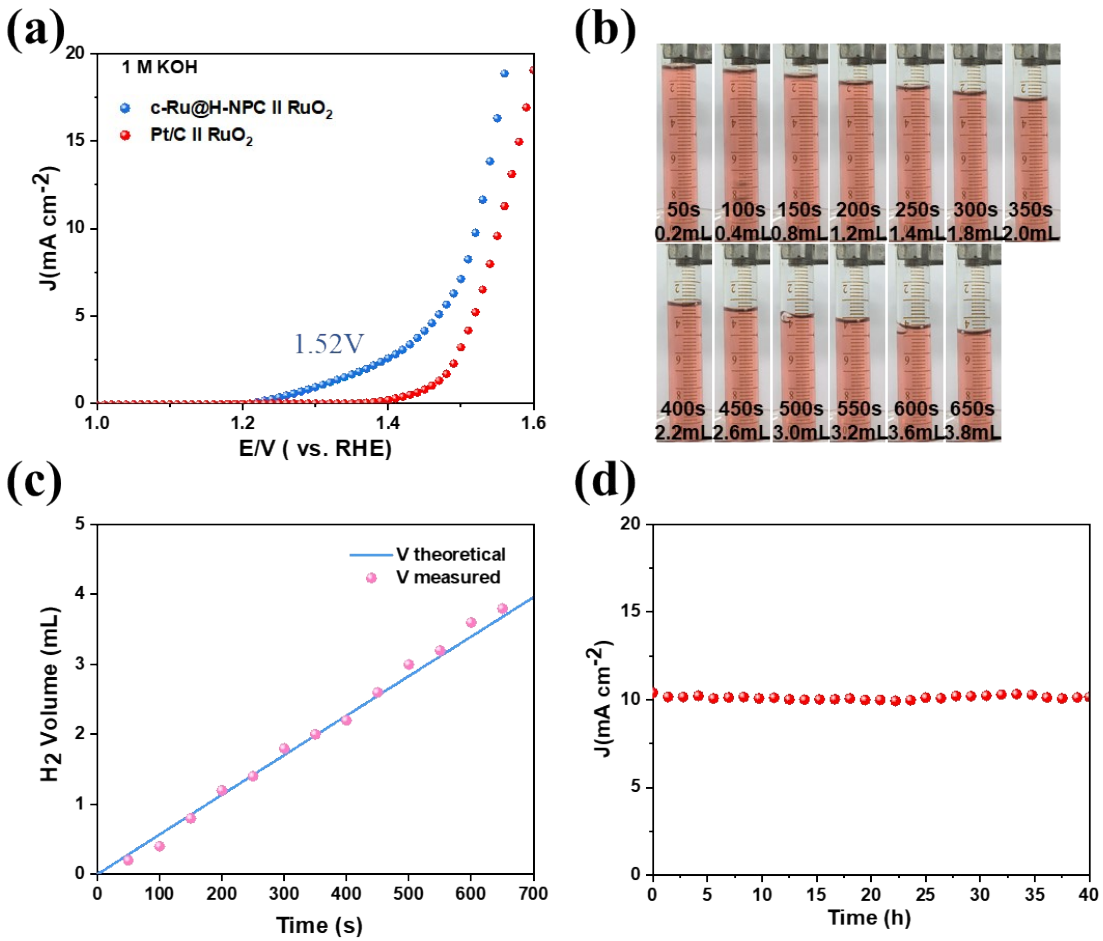

Figure S10. (a) LSV curves of two-electrode overall water splitting devices with c-Ru@H-NPC‖RuO_2; (b) digital photographs of collected H_2 in 1 M KOH; (c) measured and calculated volume of H_2; (d) i-t curve of c-Ru@H-NPC‖RuO_2 couple in 1M KOH.

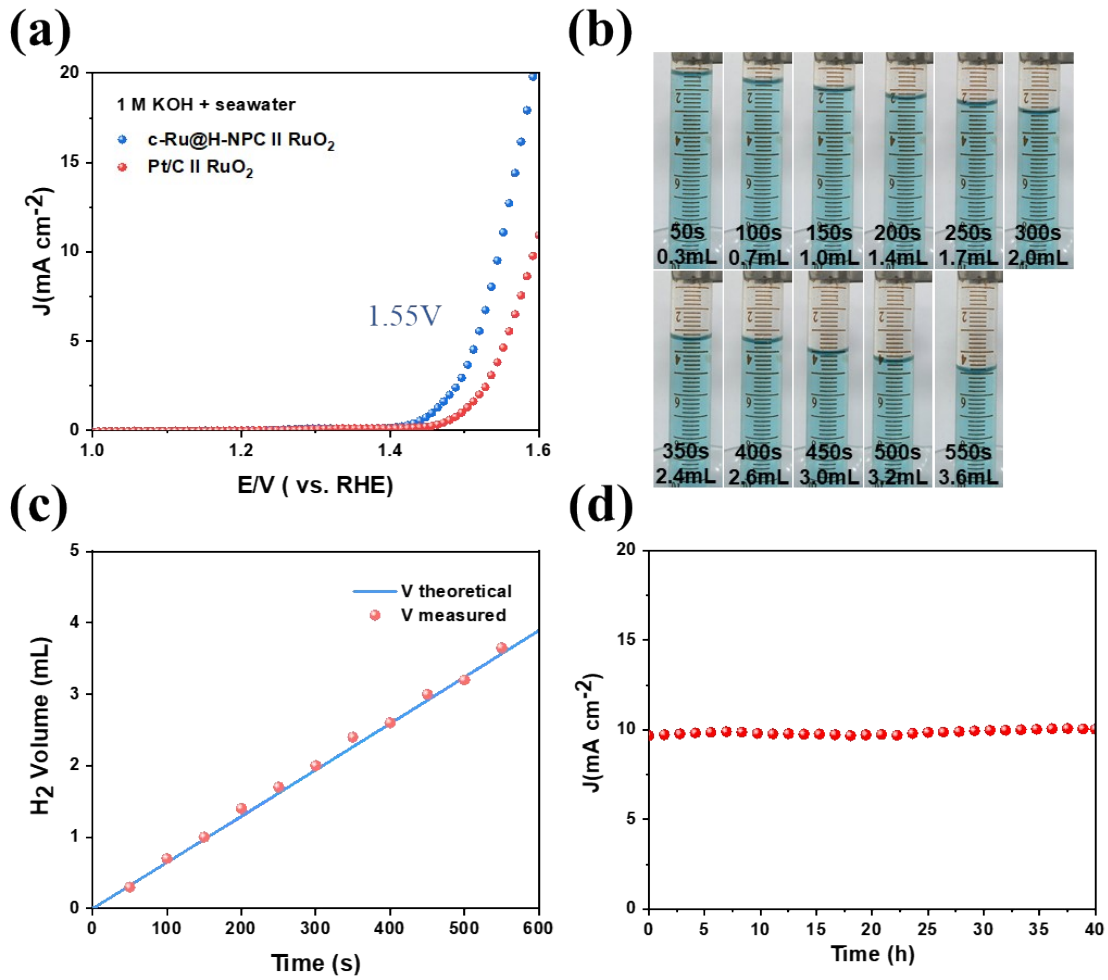

Figure S11. (a) LSV curves of two-electrode overall water splitting devices with c-Ru@H-NPC‖RuO_2; (b) digital photographs of collected H_2 in alkaline seawater; (c) measured and calculated volume of H_2 ; (d) i-t curve of c-Ru@H-NPC‖RuO_2 couple in alkaline seawater.

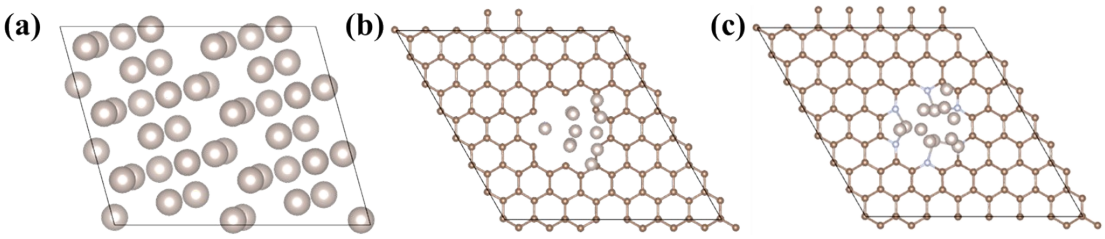

Figure S12. Theoretical models of undoped graphite supported Ru clusters, Ru/C and c-Ru@H-NPC.

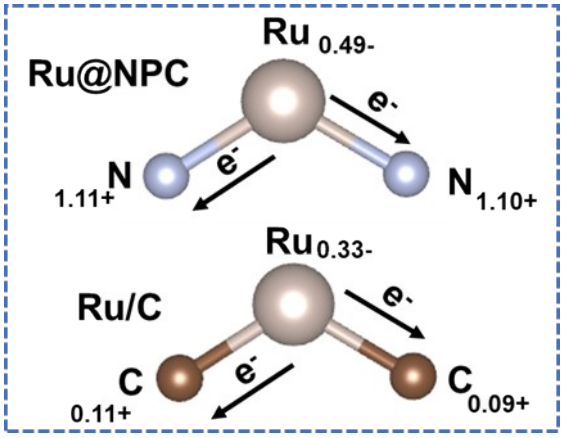

Figure S13. The difference in electron transfer between N-doped c-Ru@H-NPC and Ru/C based on Bader charge analysis.

Table S1. The specific surface area of the samples.

Sample	Surface Area(m^2/g)
UiO-66-NH_2	625
H-UiO-66-NH_2	733
H-ZrO_2/NC	259
H-NPC	1668
c-Ru@H-NPC	1438

Table S2. ICP results of catalysts.

Sample	Ru (wt.%)
c-Ru@H-NPC	4.39
c-Ru@NPC	2.49
Ru/C	5.00
c-Ru@H-NPC after test in 1 M KOH	3.97

Table S3. EXAFS fitting parameters at the Ru K-edge for Ru foil, RuO_2, c-Ru@H-NPC and c-Ru@NPC.

Sample	Scattering path	CN	R (Å)	σ^2(Å^2)	ΔE_0(eV)	R factor
Ru-foil	Ru-Ru	12	2.67±0.01	0.0027	5.7±0.8	0.0065
RuO_2	Ru-O	2	1.97±0.01	0.0051	2.9±1.0	0.0043
	Ru-Ru1	4	3.13±0.01	0.0039	2.9±1.0	
	Ru-Ru2	2	3.58±0.01	0.0033	2.9±1.0	
c-Ru@H-NPC	Ru-N/C	3.8±0.2	2.04±0.01	0.0057	6.2±1.0	0.0094
	Ru-Ru	1.4±0.2	2.69±0.01	0.0060	6.2±0.8	0.0094
c-Ru@NPC	Ru-N/C	3.8±0.2	2.03±0.01	0.0033	4.5±1.0	0.0088
	Ru-Ru	1.2±0.2	2.66±0.01	0.0033	4.5±0.8	0.0088

S_0^2 is the amplitude reduction factor; CN is the coordination number; R is interatomic distance (the bond length between central atoms and surrounding coordination atoms); σ^2 is Debye-Waller factor (a measure of thermal and static disorder in absorber-scatterer distances); ΔE_0 is edge-energy shift (the difference between the zero kinetic energy value of the sample and that of the theoretical model). R factor is used to value the goodness of the fitting. Error bounds that characterize the structural parameters obtained by EXAFS spectroscopy were estimated as N ± 20%; R ± 1%; σ^2 ± 20%.

Table S4. Comparison of HER performance with other reported Ru-based HER electrocatalysts in alkaline media.

Sample	Electrolytes	η@j (mV@ mA cm^{-2})	References
c-Ru@H-NPC	1 M KOH	10	This work
Ru/MPNC	1 M KOH	12	9
Ru NCs/NC	1 M KOH	14	10
Ru-MoS_2/CC	1 M KOH	41	11
Ru–Ru_2P/PC	1 M KOH	43.4	12
RuP_2@NPC	1 M KOH	52	13
Ru@C_2N	1 M KOH	17	14
Run-Rus/NC	1 M KOH	37	15
Ru/Co_4N-CoF_2	1 M KOH	30	16
Ru@MWCNT	1 M KOH	13	17
$Ru_xFe_{3-x}O_4$	1 M KOH	17.6	18
Ru MNSs	1 M KOH	24	19
V_O-Ru/HfO_2-OP	1 M KOH	39	20
Ru_{NP}-Ru_{SA}@CFN-800	1 M KOH	33	21
Ru@Cr-FeMOF	1 M KOH	21	22
Ru/np-MoS_2	1 M KOH	30	23
Ru/Co_3O_4 NWs	1 M KOH	30.96	24
NC@Ru_{SA}-CoP	1 M KOH	15	25
Ru/NDC	1 M KOH	28.5	26
Pd@Ru NRs	1 M KOH	30	27
Ru-NC-700	1 M KOH	12	28

Table S5. Comparison of HER performance with other reported HER electrocatalysts in simulated seawater.

Sample	Electrolytes	η@j (mV@ mA cm^{-2})	References
c-Ru@H-NPC	1 M KOH + seawater	12	This work
Ru-CoO_x/NF	1 M KOH + seawater	49	29
$RuCd_{0.02}Se_4$	1 M KOH + seawater	6.3	30
Ru-Ru_2P-4	1 M KOH + seawater	26	31
cRu-Ni_3N/NF	1 M KOH + seawater	36	32
Ru_2P@Ru/CNT	1 M KOH + seawater	29	33
NiCo@C/MXene/CF	1 M KOH + seawater	49	34
Ru_{1+NPs}/N−C	1 M KOH + seawater	58	35
l-Rh metallene	1 M KOH + seawater	38	36
Ni-SN@C	1 M KOH + seawater	23	37
$Pt_{48}Ni_{52}$	1 M KOH + seawater	51	38
RuCoBO	1 M KOH + seawater	14	39
CNFMPO	1 M KOH + seawater	73	40

C-WC-RuMg	1 M KOH + seawater	180	41
Ni-SA/NC	1 M KOH + seawater	139	42
RuSb	1 M KOH + seawater	39	43
IrO_2@MnO_2/rGO	1 M KOH + seawater	170	44
PtO_x-NiOn/NF	1 M KOH + seawater	47	45
Ag_2Se-Ag_2S-CoCH/NF	1 M KOH + seawater	75	46
CoSe/$MoSe_2$	1 M KOH + seawater	148	47
Fe-Co_2P	1 M KOH + seawater	156	48

Reference:

1 G. Kresse, J. Furthmüller, Comput. *Mater. Sci*. 1996, **6**, 15-50.

2 G. Kresse, J. Furthmüller, *Phys. Rev. B* 1996, **54**, 11169-11186.

3 M. Ernzerhof, J. P. Perdew, *J. Chem. Phys.* 1998, **109**, 3313.

4 P. E. Blöchl, *Phys. Rev. B* 1994, **50**, 17953-17979.

5 S. Grimme, J. Antony, S. Ehrlich, H. Krieg, *J. Chem. Phys*. 2010, **132**, 154104154119.

6 J. K. Nørskov, J. Rossmeisl, A. Logadottir, L. Lindqvist, J. R. Kitchin, T. Bligaard, and H. Jónsson, *J. Phys. Chem. B* 2004, **108**, 46, 17886-17892

7 J. K. Nørskov, T. Bligaard, A. Logadottir, J. R. Kitchin, J. G. Chen, S. Pandelov and U. Stimming, *J. Electrochem. Soc.* 2005, **152**, J23.

8 J. K. Norskov, F. Abild-Pedersen, F. Studt, T. Bligaard, *Proc. Natl. Acad. Sci.* 2011, **108**, 3, 937-943.

9 J. Wang, X. Guan, H. Li, S. Zeng, R. Li, Q. Yao, H. Chen, Y. Zheng and K. Qu, *Nano Energy*, 2022, **100**, 107467.

10 X. Huang, R. Lu, Y. Cen, D. Wang, S. Jin, W. Chen, I. Geoffrey, N. Waterhouse, Z. Wang, S. Tian and X. Sun, *Nano Res.*, 2023, **16**, 9073–9080.

11 D. Wang, Q. Li, C. Han, Z. Xing and X. Yang, *Appl. Catal. B*, 2019, **249**, 91–97.

12 Z. Liu, Z. Li, J. Li, J. Xiong, S. Zhou, J. Liang, W. Cai, C. Wang, Z. Yang and H. Cheng, *J. Mater. Chem. A*, 2019, **7**, 5621–5625.

13 Z. Pu, I. S. Amiinu, Z. Kou, W. Li and S. Mu, *Angew. Chem. Int. Ed.*, 2017, **129**, 11717–11722.

14 J. Mahmood, F. Li, S.-M. Jung, M. S. Okyay, I. Ahmad, S.-J. Kim, N. Park, H. Y. Jeong and J.-B. Baek, *Nature Nanotech.*, 2017, **12**, 441–446.

15 C. Yang, Z. Wu, Z. Zhao, Y. Gao, T. Ma, C. He, C. Wu, X. Liu, X. Luo, S. Li, C. Cheng and C. Zhao, *Small*, 2023, **19**, 2206949.

16 S. Zhou, H. Jang, Q. Qin, Z. Li, M. Gyu Kim, X. Ji, X. Liu and J. Cho, *Chem. Eng. J*, 2021, **414**, 128865.

17 D. H. Kweon, M. S. Okyay, S.-J. Kim, J.-P. Jeon, H.-J. Noh, N. Park, J. Mahmood and J.-B. Baek, *Nat. Commun.*, 2020, **11**, 1278.

18 X. Mu, X. Zhang, Z. Chen, Y. Gao, M. Yu, D. Chen, H. Pan, S. Liu, D. Wang and S. Mu, *Nano Lett.*, 2024, **24**, 1015–1023.

19 J. Zhang, X. Mao, S. Wang, L. Liang, M. Cao, L. Wang, G. Li, Y. Xu and X. Huang, *Angew. Chem. Int. Ed.*, 2022, **61**, e202116867.

20 G. Li, H. Jang, S. Liu, Z. Li, M. G. Kim, Q. Qin, X. Liu and J. Cho, *Nat. Commun.*, 2022, **13**, 1270.

21 T. Luo, J. Huang, Y. Hu, C. Yuan, J. Chen, L. Cao, K. Kajiyoshi, Y. Liu, Y. Zhao, Z. Li and Y. Feng, *Adv. Funct. Mater.*, 2023, **33**, 2213058.

22 C. Zhao, J. Wang, Y. Gao, J. Zhang, C. Huang, Q. Shi, S. Mu, Q. Xiao, S. Huo, Z. Xia, J. Zhang, X. Lu and Y. Zhao, *Adv. Funct. Mater.*, 2024, **34**, 2307917.

23 K. Jiang, M. Luo, Z. Liu, M. Peng, D. Chen, Y.-R. Lu, T.-S. Chan, F. M. F. De Groot and Y. Tan, *Nat. Commun.*, 2021, **12**, 1687.

24 Z. Liu, L. Zeng, J. Yu, L. Yang, J. Zhang, X. Zhang, F. Han, L. Zhao, X. Li, H. Liu and W. Zhou, *Nano Energy*, 2021, **85**, 105940.

25 Z. Wang, K. Chi, S. Yang, J. Xiao, F. Xiao, X. Zhao and S. Wang, *Small*, 2023, **19**, 2301403.

26 J.-T. Ren, L. Chen, H.-Y. Wang, W.-W. Tian, X. Zhang, T.-Y. Ma, Z. Zhou and Z.-Y. Yuan, *Appl. Catal. B*, 2023, **327**, 122466.

27 Y. Luo, X. Luo, G. Wu, Z. Li, G. Wang, B. Jiang, Y. Hu, T. Chao, H. Ju, J. Zhu, Z. Zhuang, Y. Wu, X. Hong and Y. Li, *ACS Appl. Mater. Interfaces*, 2018, **10**, 34147–34152.

28 B. Lu, L. Guo, F. Wu, Y. Peng, J. E. Lu, T. J. Smart, N. Wang, Y. Z. Finfrock, D. Morris, P. Zhang, N. Li, P. Gao, Y. Ping and S. Chen, *Nat Commun*, 2019, **10**, 631.

29 D. Wu, D. Chen, J. Zhu and S. Mu, *Small*, 2021, **17**, 2102777.

30 X. Gu, M. Yu, S. Chen, X. Mu, Z. Xu, W. Shao, J. Zhu, C. Chen, S. Liu and S. Mu, *Nano Energy*, 2022, **102**, 107656.

31 D. Chen, R. Yu, R. Lu, Z. Pu, P. Wang, J. Zhu, P. Ji, D. Wu, J. Wu, Y. Zhao, Z. Kou, J. Yu and S. Mu, *InfoMat*, 2022, **4**, e12287.

32 J. Zhu, R. Lu, W. Shi, L. Gong, D. Chen, P. Wang, L. Chen, J. Wu, S. Mu and Y. Zhao, *Energy Environ. Mater.*, 2023, **6**, e12318.

33 D. Zhang, H. Miao, X. Wu, Z. Wang, H. Zhao, Y. Shi, X. Chen, Z. Xiao, J. Lai and L. Wang, *Chinese Chinese J. Catal.*, 2022, **43**, 1148–1155.

34 F. Sun, J. Qin, Z. Wang, M. Yu, X. Wu, X. Sun and J. Qiu, *Nat Commun*, 2021, **12**, 4182.

35 S. Wang, M. Wang, Z. Liu, S. Liu, Y. Chen, M. Li, H. Zhang, Q. Wu, J. Guo, X. Feng, Z. Chen and Y. Pan, *ACS Appl. Mater. Interfaces*, 2022, **14**, 15250–15258.

36 K. Deng, Q. Mao, W. Wang, P. Wang, Z. Wang, Y. Xu, X. Li, H. Wang and L. Wang, *Appl. Catal. B*, 2022, **310**, 121338.

37 H. Jin, X. Wang, C. Tang, A. Vasileff, L. Li, A. Slattery and S. Qiao, *Adv. Mater.,* 2021, **33**, 2007508.

38 X. Zhang, Y. Xiao, G. Tian, X. Yang, Y. Dong, F. Zhang and X. Yang, *Chem. Eur. J*, 2023, **29**, e202202811.

39 L.-W. Shen, Y. Wang, J.-B. Chen, G. Tian, K.-Y. Xiong, C. Janiak, D. Cahen and X.-Y. Yang, *Nano Lett.*, 2023, **23**, 1052–1060.

40 H.-M. Zhang, L. Zuo, Y. Gao, J. Guo, C. Zhu, J. Xu and J. Sun, *J Mater. Sci. Technol.*, 2024, **173**, 1–10.

41 H. Wu, Z. Zhao, M. Wang, W. Zheng, Y. Zhang, Y. Wang, T. Ma, Z. Zeng, C. Cheng and S. Li, *J. Mater. Chem. A*, 2024, **12**, 10755–10763.

42 W. Zang, T. Sun, T. Yang, S. Xi, M. Waqar, Z. Kou, Z. Lyu, Y. P. Feng, J. Wang and S. J. Pennycook, *Adv. Mater.*, 2021, **33**, 2003846.

43 X. Liu, T. Wang, Y. Chen, J. Wang, W. Xie, R. Wu, X. Xu, L. Pang, X. Zhang, Y. Lv, G. Wang, Y. Yamauchi and T. (Leo) Jin, *Appl. Catal. B*, 2023, **333**, 122771.

44 S. C. Karthikeyan, R. Santhosh Kumar, S. Ramakrishnan, S. Prabhakaran, A. R. Kim, D. H. Kim and D. J. Yoo, *ACS Sustainable Chem. Eng.*, 2022, **10**, 15068–15081.

45 W. Yu, H. Liu, Y. Zhao, Y. Fu, W. Xiao, B. Dong, Z. Wu, Y. Chai and L. Wang, *Nano Res.*, 2023, **16**, 6517–6530.

46 L. Yang, C. Feng, C. Guan, L. Zhu and D. Xia, *Appl. Surf. Sci.*, 2023, **607**, 154885.

47 J. Sun, J. Li, Z. Li, C. Li, G. Ren, Z. Zhang and X. Meng, *ACS Sustainable Chem. Eng.*, 2022, **10**, 9980–9990.

48 Y. Lin, K. Sun, X. Chen, C. Chen, Y. Pan, X. Li and J. Zhang, *J. Energy Chem.*, 2021, **55**, 92–101.